COMMUNICATIONS IN COMPUTATIONAL PHYSICS
Vol. **3**, No. 1, pp. 63-84

Commun. Comput. Phys.
January 2008

Direct Simulation Methods for Scalar-Wave Envelopes in Two-Dimensional Layered Random Media Based on the Small-Angle Scattering Approximation

Tatsuhiko Saito[1,2,*], Haruo Sato[3] and Tsutomu Takahashi[4]

[1] *Earthquake Research Institute, The University of Tokyo, Yayoi 1-1-1, Bunkyo-ku, Tokyo, 113-0032, Japan.*
[2] *CREST, Japan Science and Technology Agency (JST).*
[3] *Department of Geophysics, Graduate School of Science, Tohoku University, Aramaki-Aza-Aoba 6-3, Aoba-ku, Sendai, Miyagi, 980-8578, Japan.*
[4] *Institute for Research on Earth Evolution, Japan Agency for Marine-Earth Science and Technology, Showa-machi 3173-25, Kanazawa-ku, Yokohama, Kanagawa, 236-0001, Japan.*

Received 1 September, 2006; Accepted (in revised version) 6 June, 2007

Available online 14 September 2007

Abstract. This study presents stochastic methods to simulate wave envelopes in layered random media. High-frequency Seismograms of small earthquakes are so complex due to lithospheric inhomogeneity that seismologists often analyze wave envelopes rather than wave traces to quantify the subsurface inhomogeneity. Since the statistical properties of the inhomogeneity vary regionally, it is important to develop and examine direct envelope simulation methods for non-uniform random media. As a simple example, this study supposes plane wave propagation through two-layer random media in 2-D composed of weak and strong inhomogeneity zones. The characteristic spatial-scale of the inhomogeneity is supposed to be larger than the wavelength, where small-angle scattering around the forward direction dominates large-angle scattering. Two envelope simulation methods based on the small-angle scattering approximation are examined. One method is to solve a differential equation for the two-frequency mutual coherence function with the Markov approximation. The other is to solve the stochastic ray bending process by using the Monte Carlo method based on the Markov approximation for the mutual coherence function. The resultant wave envelopes of the two methods showed excellent coincidence both for uniform and for two-layer random media. Furthermore, we confirmed the validity of the two methods comparing with the envelopes made from the finite difference simulations of waves. The two direct envelope simulation methods presented in this study can be a mathematical base for the study of high-frequency wave propagation through randomly inhomogeneous lithosphere in seismology.

*Corresponding author. *Email addresses:* saito-ta@eri.u-tokyo.ac.jp (T. Saito), sato@zisin.geophys.tohoku.ac.jp (H. Sato), ttaka@jamstec.go.jp (T. Takahashi)

 ©2008 Global-Science Press

AMS subject classifications: 86A15

Key words: Seismic wave, envelope, random media.

1 Introduction

High-frequency seismic-wave propagation through the earth shows highly complicated behavior because of medium heterogeneity. We see numerous phases in addition to direct P- and S-waves, and S-wave trains are formed around direct S-waves in seismograms of small earthquakes (Fig. 1). Most of the phases are interpreted as waves scattered by random inhomogeneities distributed in lithosphere. Accepting the complexity of the seismograms, seismologists often investigate wave envelopes instead of wave traces to quantify medium inhomogeneity. Observed envelopes show systematic behavior related to the travel distance and the wave frequency [15, 25]. The behavior is strongly governed by the statistical properties of the medium inhomogeneity.

In seismology, there are some approaches for simulating directly wave envelopes without calculating wave traces based on the statistical information such as the power spectrum density function (PSDF) or the auto correlation function (ACF) of medium fractional fluctuation. We refer to such approaches as direct envelope simulation methods. The radiative transfer theory is one of the methods to simulate the envelopes of coda waves [e.g., 1, 3]. The heuristic approach to the radiative transfer theory and its application to seismology are summarized in [28]. Theoretical derivation of the radiative transfer equation based on the Bethe-Salpeter equation for waves through random media is well summarized in [12]. The validity of the radiative transfer theory with the Born approximation is examined carefully by a comparison with numerical finite-difference simulations [18, 38].

Another typical method for the direct envelope simulation is based on a statistical method called the Markov approximation which supposes small-angle scattering around the forward direction. This method was originally developed for optical waves in radio physics [9, 20, 32, 36], and may be considered as a stochastic extension of the split step method for the parabolic wave equation [8, 34]. The validity of the Markov approximation can be examined by a comparison between the envelope of the Markov approximation and the averaged envelopes which are made from the numerically calculated wave traces [2]. Employing the method of the Markov approximation, H. Sato simulated envelopes of S-wave trains, or S-wave envelopes, and showed the duration of the envelopes increases with increasing the travel distance [25]. It is consistent with the observation that S-wave trains of small earthquakes usually show the increase in the duration as shown in Fig. 1. Following this study, many studies have applied the method for the interpretation of high-frequency seismograms [15, 16, 24, 30, 35]. In parallel with the application to observed seismograms, theoretical simulation methods have also been developed to adopt more realistic conditions for the lithospheric inhomogeneity. The original method

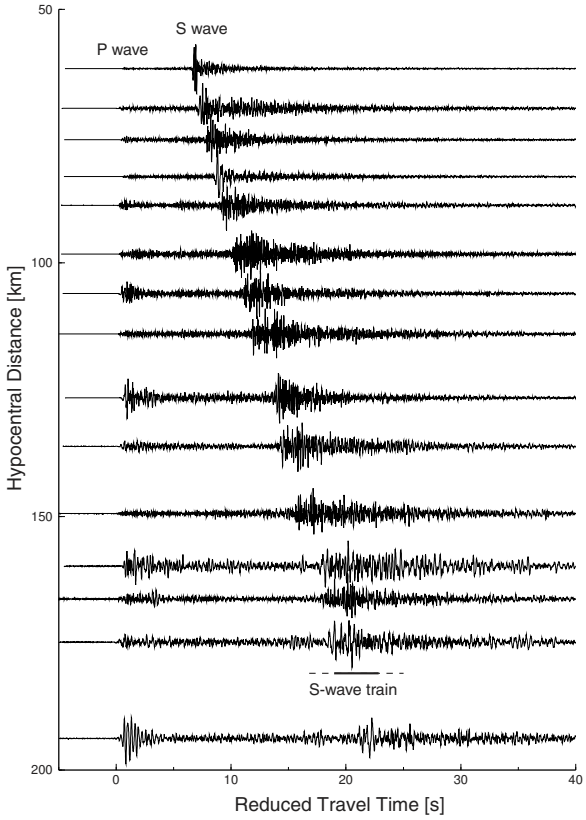

Figure 1: Variation of transverse-component seismograms (2-32 Hz band) of a local earthquake of M 4.0 with increasing travel distance. Data are registered by Hi-net. Traces are plotted against reduced travel time with the velocity of 7km/s.

supposed the random media characterized by a Gaussian ACF without intrinsic absorption since this ACF is mathematically easily tractable [32, 33]. In seismology, intrinsic absorption was phenomenologically introduced [25], and a power-law type PSDF was introduced for characterizing more realistic random media [22]. Also, a simulation method of envelopes in 2-D weakly anisotropic random media was successfully formulated [21]. Recently, a method of elastic vector-wave envelopes having radial and transverse components was proposed [10, 26, 27]. To include large-angle scattering in the framework, combined methods of the Markov approximation and the radiative transfer theory were proposed [23, 29].

One of the most attractive topics in seismology is to image a spatial variation of the statistical properties in the earth medium. For example, medium inhomogeneities are different between the crust and mantle [19]. In Japan, high-frequency S-wave trains show systematic change related to the volcanic front due to the non-uniform statistical properties of the inhomogeneity [4, 15] and non-uniform absorption structure [42]. Recently, anomalous scattering bodies beneath Quaternary volcanoes were successfully imaged by

analyzing a large number of S-wave envelopes recorded by high-sensitivity seismograph network Japan (Hi-net) [35]. As the mathematical basis of those studies, envelopes in random media characterized by non-uniform statistical properties should be examined. The envelope simulations based on the radiative transfer theory [5, 6, 7, 14, 41] and on the diffusion equation [37] have been investigated for the case of non-uniform random media. However, there have been few studies on the envelope synthesis of the Markov approximation in non-uniform random media.

This study presents direct envelope simulation methods for plane-wave propagation in two-layer random media in 2-D as the simplest case for non-uniform random media. In Section 2, we numerically calculate wave envelopes in two-layer random media for the incidence of a plane wavelet with the finite-difference (FD) method to obtain reference envelopes that will be compared with the envelopes of the two direct simulation methods. In Section 3, solving a differential equation for the two-frequency mutual coherence function with the Markov approximation, we obtain wave envelopes. In Section 4, we describe another direct envelope simulation method which uses the Monte Carlo method to simulate ray bending process in scattering media, which is based on the Markov approximation for the mutual coherence function. In Section 5, we compare the envelopes obtained by the two direct simulation methods with the FD envelopes to validate these methods. Finally, in Section 6, we summarize our study.

2 Plane-wave propagation in two-layer random media in two-dimensional space: FD envelopes

We consider propagation of a scalar wave $u(\mathbf{x},t)$ through inhomogeneous media in 2-D space governed by

$$\left(\Delta-\frac{1}{V(\mathbf{x})^2}\frac{\partial^2}{\partial t^2}\right)u(\mathbf{x},t)=0, \tag{2.1}$$

where $\mathbf{x}=(x,z)$ and Δ is the Laplacian. In randomly inhomogeneous media, the velocity is written as

$$V(\mathbf{x})=V_0\{1+\xi(\mathbf{x})\},$$

where the fractional velocity fluctuation $\xi(\mathbf{x})$ is a random function of location $\mathbf{x}$ and is small $|\xi|\ll 1$. We consider an ensemble of the fractional fluctuation $\{\xi(\mathbf{x})\}$ such that $\langle\xi(\mathbf{x})\rangle=0$, where the angular brackets mean the ensemble average. The media are referred to as random media which are statistically characterized by an ACF $R(\mathbf{x}_d)=\langle\xi(\mathbf{x}+\mathbf{x}_d)\xi(\mathbf{x})\rangle$. This study supposes that $\xi(\mathbf{x})$ is statistically homogeneous and isotropic in a layer, and is characterized by a Gaussian ACF as

$$R(x_d)=\varepsilon^2\exp\left(-x_d^2/a^2\right), \tag{2.2}$$

where ε is the root-mean-square value of the fractional velocity fluctuation and a is the correlation distance which is a characteristic scale-length of the inhomogeneity. The cor-

responding PSDF in 2-D space is given by

$$P(m)=\int_{-\infty}^{\infty}\int_{-\infty}^{\infty}R(\mathbf{x_d})\exp(-i\mathbf{m}\cdot\mathbf{x_d})d\mathbf{x_d}=\pi\varepsilon^2a^2\exp\left(-\frac{m^2a^2}{4}\right), \tag{2.3}$$

where $\mathbf{m}$ is the wavenumber vector and $m=|\mathbf{m}|$.

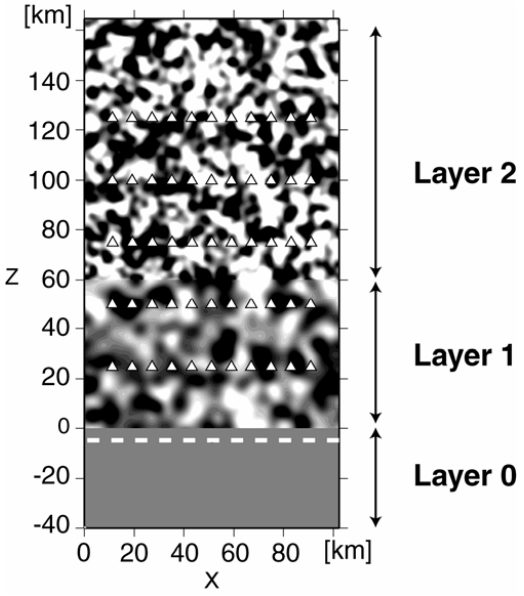

Figure 2: Geometry of a two-layer random medium and line receiver arrays (triangles) in 2-D space for finite difference (FD) simulations. Two-layer random medium is composed of Layer 1 (weak inhomogeneity zone, ε=0.04, a=5km, 0km$<z<$60km) and Layer 2 (strong inhomogeneity zone, ε=0.07, a=3km, 60km$<z<$160km). Plane Ricker wavelet with 2Hz dominant frequency is generated from a white dashed line ($z=-5$km) in Layer 0 (gray area, -40km$<z<$0km).

We first numerically study the wave propagation through two-layer random media (Fig. 2) for the incidence of a plane wavelet by using the finite difference (FD) method. Layer 0 between $z=-40$km and 0 km is homogenous, characterized by the background velocity $V_0=4$km/s. Layer 1 between $z=0$ and 60km has weak inhomogeneity characterized by RMS fractional fluctuation $\varepsilon=0.04$ and correlation distance $a=5$km. Layer 2 between $z=60$ and 160km has strong inhomogeneity characterized by $\varepsilon=0.07$, $a=3$km. For the realization of a random medium, we generate random numbers and distribute them on a 2-D grid space, thus producing random fluctuation with a white-noise type PSDF. We then take the Fourier transform of the random fluctuation, correct the spectrum amplitude according to Eq. (2.3), take the inverse Fourier transform, and we get $\xi(\mathbf{x})$. A plane wavelet is generated at $z=-5$km in Layer 0. We use a Ricker wavelet with the dominant frequency f_c=2Hz as a source time function. The plane wavelet propagates along the z-axis and plunges into Layer 1. Line receiver arrays are put at $z=25$, 50, 75, 100 and 125km; each line array consists of 11 receivers with 8km spacing along the x-axis.

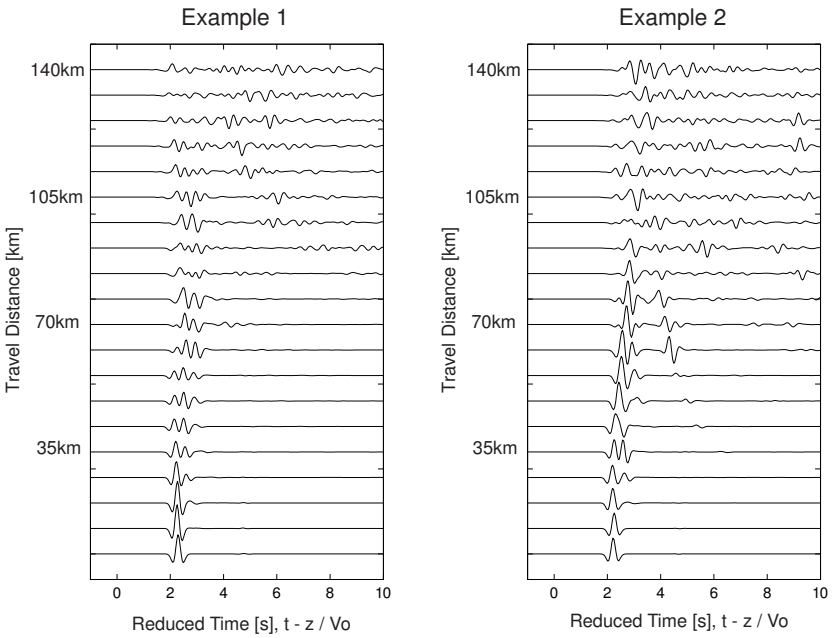

Figure 3: Wave traces at different travel distances in two realizations of the two-layer random media by using the FD simulations for the incidence of a 2Hz Ricker wavelet. The traces are plotted against reduced travel time with velocity $V_0 = 4$km/s.

The first and the second line arrays are located in Layer 1, and the third, fourth and fifth line arrays are in Layer 2. We numerically solve the wave propagation by the FD method with fourth-order accuracy in space and second-order one in time with grid spacing of 50m and time step of 4ms [21]. Absorbing boundary condition is set at the both ends orthogonal to the z-axis, and periodic boundary condition is set at the both ends orthogonal to the x-axis. As examples, Fig. 3 shows wave traces at different travel distances in two realizations of the random media. Increasing the travel distance, wave traces become complex to contain more number of phases. However, the maximum amplitude does not always decrease with increasing the travel distance.

To investigate the statistical properties of the wavefield, we synthesize mean-square (MS) envelopes from 20 realizations of the random media having the same PSDFs as follows. At first, we calculate an envelope at each station by using the Hilbert transform [31]. Then, the envelopes of 11 receivers on a line array are squared and averaged to obtain squared envelopes for a single realized medium. Finally, the squared envelopes in 20 realized random media are averaged to obtain MS envelopes. They are referred to as FD envelopes, hereinafter. Fig. 4a shows the FD envelopes [bold gray curves] at the travel distance $z = 25$, 50, 75, 100 and 125km in the two-layer random media. Dashed curves around the bold gray curve indicate the standard deviation of the FD envelopes. The standard deviation is estimated by a bootstrap method, in which MS envelopes are repeatedly replicated from 20 envelopes randomly taken with replacement from the com-

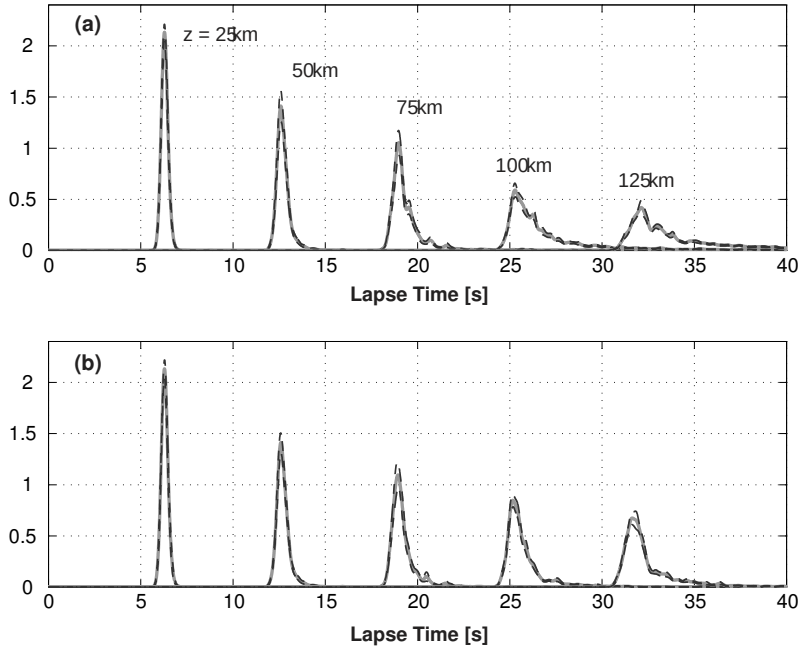

Figure 4: Mean-square (MS) envelopes (gray curves) in (a) the two-layer random media and (b) uniform random media (ε=0.04, a=5km, 0km$<z<$160km) by using finite-difference simulations (FD envelopes) for the incidence of a 2Hz Ricker wavelet. Black dashed curves indicate the range of one standard deviation of the FD envelopes.

plete set of the original envelopes. The FD envelopes indicate that the maximum amplitude smoothly decreases with increasing the travel distance, although it is difficult to see such systematic variation in wave traces in each individual realization as shown in Fig. 3. The amplitude attenuation is due to wave scattering (scattering attenuation) caused by medium inhomogeneity since our simulation considers neither intrinsic absorption nor geometrical spreading. Furthermore, the duration of the envelope increases with increasing the travel distance. This feature is referred to as envelope broadening, that is observed in S-wave envelopes of small earthquakes [25]. As a comparison, Fig. 4b shows plots of FD envelopes for the uniform random media characterized by the weak inhomogeneity [$\varepsilon = 0.04$, $a = 5$km, $0 < z < 160$km]. Due to the lack of a strong inhomogeneity zone, the maximum amplitude in Fig. 4b decreases more slowly with travel distance than that in Fig. 4a.

3 Markov envelopes

We describe the direct envelope synthesis method by using the Markov approximation where a differential equation of two-frequency mutual coherence function is solved. This study deals with the wave propagation through random media for the incidence of a plane wavelet in 2-D space; the derivation is similar to the study [10]. Wavefield $u(x,z,t)$

in 2-D space is written as a superposition of harmonic plane waves of angular frequency ω as

$$u(x,z,t)=\frac{1}{2\pi}\int_{-\infty}^{\infty}d\omega\, U(x,z,\omega)e^{i(kz-\omega t)}, \tag{3.1}$$

where the wavenumber $k=\omega/V_0$. When the wavelength is smaller than the correlation distance of the medium inhomogeneity $ak\gg 1$, we may neglect the second derivative of $U(x,z,\omega)$ with respect to the direction z and obtain the parabolic wave equation

$$2ik_0\frac{\partial U}{\partial z}+\frac{\partial^2 U}{\partial x^2}-2k_0^2\xi U=0. \tag{3.2}$$

In order to derive the MS envelope, we introduce a two-frequency mutual coherence function (TFMCF). The TFMCF is defined as an ensemble average of a product of wavefields at two points x' and x'' on the x-axis and two angular frequencies ω' and ω'' at the travel distance z,

$$\Gamma_2\left(x',x'',z,\omega',\omega''\right)\equiv\left\langle U\left(x',z,\omega'\right)U\left(x'',z,\omega''\right)^*\right\rangle, \tag{3.3}$$

where the asterisk denotes complex conjugate. When a plane wave propagates along the z-axis (Fig. 2), Γ_2 is dependent only on $x_d=x'-x''$, but is independent of $x_c=(x'+x'')/2$, since the random media are statistically homogeneous along the x-axis. Introducing central angular-frequency $\omega_c=(\omega_1+\omega_2)/2$ and difference angular-frequency $\omega_d=\omega_1-\omega_2$, we explicitly write arguments of Γ_2 as $\Gamma_2(x_d,z,\omega_d,\omega_c)$. Then, the intensity of the wavefield is written as

$$\begin{aligned}I(z,t)\equiv\left\langle|u(x,z,t)|^2\right\rangle&=\frac{1}{(2\pi)^2}\int_{-\infty}^{\infty}\int_{-\infty}^{\infty}d\omega_c d\omega_d\Gamma_2(x_d=0,z,\omega_d,\omega_c)\exp\{-i\omega_d(t-z/V_0)\}\\&=\frac{1}{2\pi}\int_{-\infty}^{\infty}d\omega_c\hat{I}(z,t;\omega_c),\end{aligned} \tag{3.4}$$

where the intensity spectral density function $\hat{I}(z,t;\omega_c)$ is given by

$$\hat{I}(z,t;\omega_c)\equiv\frac{1}{2\pi}\int_{-\infty}^{\infty}d\omega_d\Gamma_2(x_d=0,z,\omega_d,\omega_c)\exp\{-i\omega_d(t-z/V_0)\}. \tag{3.5}$$

We may interpret $\hat{I}(z,t;\omega_c)\Delta\omega$ as the MS envelope of the bandpass-filtered trace with the center frequency ω_c and a bandwidth $\Delta\omega$. In order to obtain Γ_2 at a travel distance $z=Z_0$, the master equation is derived from Eq. (3.2) as

$$\frac{\partial\Gamma_2}{\partial z}+i\frac{k_d}{2k_c^2}\frac{\partial^2\Gamma_2}{\partial x_d^2}+k_c^2[A(0)-A(x_d)]\Gamma_2+\frac{k_d^2}{2}A(0)\Gamma_2=0, \tag{3.6}$$

where a function A is given by

$$A(x_d) \equiv \int_{-\infty}^{\infty} R(x_d,z_d)\,dz_d = \sqrt{\pi}\varepsilon^2 a \exp\left(-x_d^2/a^2\right)$$
$$\approx \sqrt{\pi}\varepsilon^2 a\left(1-x_d^2/a^2\right) \quad \text{for} \quad |x_d| << a\,, \tag{3.7}$$

for the Gaussian ACF [2]. In the derivation of Eq. (3.6), we supposed quasi-monochromatic waves of central wavenumber $k_c = (k'+k'')/2$ and difference wavenumber $k_d = k'-k''$. In Eq. (3.7), the approximation $|x_d| \ll a$ is used, since the correlation of the wavefield at two points spatially separated on the transverse axis rapidly decreases to zero with increasing the lag distance [see p. 245, 28]. The value of Γ_2 is written as the following product

$$\Gamma_2 = {}_0\Gamma_2 \exp\left(-\frac{\omega_d^2 A(0) z}{2V_0^2}\right). \tag{3.8}$$

The Fourier transform of the exponential term in Eq. (3.8) is given by

$$w(z,t) = \frac{1}{2\pi}\int_{-\infty}^{\infty} d\omega_d \exp\left(-\frac{A(0)z\omega_d^2}{2V_0^2}\right)\exp(-i\omega_d t)$$
$$= \frac{V_0}{\sqrt{2\pi A(0)z}}\exp\left(-\frac{V_0^2 t^2}{2A(0)z}\right). \tag{3.9}$$

The function $w(z,t)$ shows the wandering effect which corresponds to the probabilistic distribution of the onset time estimated from the geometrical optics [e.g. 11]; the variance of the onset time is given by $A(0)z/{V_0}^2$ on the basis of the geometrical optics [see Eq. (8.24), 28]. The intensity spectral density function (3.5) is then given by a convolution form as

$$\hat{I}(z,t;\omega_c) = \int_{-\infty}^{\infty} dt' w\left(z,t-t'\right)\hat{I}_0\left(z,t';\omega_c\right), \tag{3.10}$$

where

$$\hat{I}_0(z,t;\omega_c) = \frac{1}{2\pi}\int_{-\infty}^{\infty} d\omega_d {}_0\Gamma_2\left(x_d=0,z,\omega_d,\omega_c\right)\exp\left\{-i\omega_d\left(t-z/V_0\right)\right\}. \tag{3.11}$$

From Eqs. (3.6) and (3.8), the master equation for ${}_0\Gamma_2$ is given by

$$\frac{\partial {}_0\Gamma_2\left(x_d,z,\omega_c,\omega_d\right)}{\partial z} + i\frac{k_d}{2k_c^2}\frac{\partial^2 {}_0\Gamma_2}{\partial x_d^2} + \sqrt{\pi}\varepsilon^2 k_c^2 a\left(\frac{x_d^2}{a^2}\right){}_0\Gamma_2 = 0 \tag{3.12}$$

for the case of the Gaussian ACF. In order to solve Eq. (3.12) in the two-layer random media, we take the x_d- and z-axes as shown in Fig. 5a. Layer 1 ranges between $z=0$ and

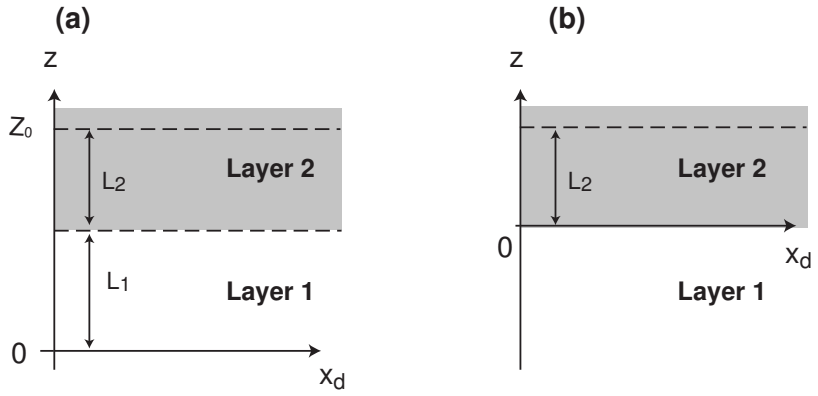

Figure 5: Coordinate used for the envelope synthesis using the Markov approximation. The z- and z'-axes are in the global ray direction of a plane wave, and the x_d-axis is orthogonal to the z-axis. The distance L_1 is the travel distance in Layer 1, and L_2 is that in Layer 2. The total travel distance is Z_0.

L_1, and the Layer 2 ranges $z > L_1$. We calculate ${}_0\Gamma_2(x_d,Z_0,\omega_c,\omega_d)$ at a travel distance Z_0 with respect to the initial condition ${}_0\Gamma_2(x_d,0,\omega_d,\omega_c)=1$ which corresponds to $\hat{I}(0,t;\omega_c)=\delta(t)$. Considering the symmetry of ${}_0\Gamma_2$ with respect to the x_d-axis, we set the boundary condition at $x_d=0$ as

$$\partial_0\Gamma_2(x_d,z,\omega_c,\omega_d)/\partial x_d\big|_{x_d=0}=0.$$

For the case that the travel distance Z_0 is smaller than L_1, Eq. (3.12) is solved analytically [10]. Setting the medium parameters in Layer 1 as ε_1 and a_1, and introducing a characteristic time

$$t_M=\frac{\sqrt{\pi}\varepsilon_1^2 Z_0^2}{2V_0 a_1}, \tag{3.13}$$

the solution is given by

$${}_0\Gamma_2(x_d,Z_0,\omega_d,\omega_c)=\frac{\exp\left\{-\frac{\tan(s_0\tau)}{s_0}\chi^2\right\}}{\sqrt{\cos(s_0\tau)}}, \tag{3.14}$$

where

$$\tau=z/Z_0,\quad \chi=\sqrt{2Z_0V_0k_c^2t_M}\,x_d/Z_0,\quad s_0=2\sqrt{t_M\omega_d}\exp(i\pi/4).$$

Using this solution, we obtain the solution at the end of Layer 1, ${}_0\Gamma_2(x_d,L_1,\omega_d,\omega_c)$.

Then, we consider the propagation in Layer 2 introducing the z'-axis whose origin is located at $z=L_1$ (Fig. 5b). The solution ${}_0\Gamma_2(x_d,z=L_1,\omega_d,\omega_c)$ in Layer 1 is used as an initial condition ${}_0\Gamma_2(x_d,z'=0,\omega_d,\omega_c)$ in Layer 2. The situation is similar to the propagation in Layer 1, but the difference is that the initial condition in Layer 2 is not constant, ${}_0\Gamma_2(x_d,z'=0,\omega_d,\omega_c)\neq 1$. Because of this initial condition, we cannot use an analytical solution like Eq. (3.14). We solve the Eq. (3.12) in Layer 2 numerically. The characteristic time in Layer 2 is given by

$$t_M=\frac{\sqrt{\pi}\varepsilon_2^2 L_2^2}{2V_0 a_2}. \tag{3.15}$$

Introducing two non-dimensional parameters as

$$\mu=\frac{(t_M\omega_d)^{1/2}}{L_2}z',\quad \nu=(t_M\omega_d)^{-1/4}\frac{\sqrt{2L_2V_0k_c^2t_M}}{L_2}x_d, \tag{3.16}$$

we rewrite Eq. (3.12) as

$$\frac{\partial_0\Gamma_2(\nu,\mu)}{\partial\mu}+i\frac{\partial^2{}_0\Gamma_2}{\partial\nu^2}+\nu^2{}_0\Gamma_2=0. \tag{3.17}$$

Also, the initial condition ${}_0\Gamma_2(x_d,z'=0,\omega_d,\omega_c)$ is rewritten as ${}_0\Gamma_2(\nu,0)$. To obtain the solution ${}_0\Gamma_2(x_d,z'=L_2,\omega_d,\omega_c)$, we estimate $\Gamma_2(\nu,\sqrt{t_M\omega_d})$ by solving Eq. (3.17) numerically. Using a finite difference expression ${}_0\Gamma_2(\nu_j,\mu_n)={}_0\Gamma_2|_j^n$ and employing Crank-Nicholson scheme [17], we obtain a finite difference equation from Eq. (3.17),

$$\begin{aligned}&\frac{i\Delta\mu}{2(\Delta\nu)^2}\Gamma|_{j+1}^{n+1}+\left\{1-\frac{i\Delta\mu}{(\Delta\nu)^2}+\frac{\Delta\mu\nu_j}{2}\right\}\Gamma|_j^{n+1}+\frac{i\Delta\mu}{2(\Delta\nu)^2}\Gamma|_{j-1}^{n+1}\\&=-\frac{i\Delta\mu}{2(\Delta\nu)^2}\Gamma|_{j+1}^{n}+\left\{1+\frac{i\Delta\mu}{(\Delta\nu)^2}-\frac{\Delta\mu\nu_j}{2}\right\}\Gamma|_j^{n}-\frac{i\Delta\mu}{2(\Delta\nu)^2}\Gamma|_{j-1}^{n}.\end{aligned} \tag{3.18}$$

We calculate ${}_0\Gamma_2|_j^n$ from ${}_0\Gamma_2|_j^{n-1}$ using Eq. (3.18), where the range [0, 8] is discretized with the grid size $\Delta\nu=0.02$ on the ν axis and the grid step is $\Delta\mu=0.02$ on the μ axis. The boundary conditions are set as ${}_0\Gamma_2|_0^n={}_0\Gamma_2|_1^n$ and ${}_0\Gamma_2|_J^n={}_0\Gamma_2|_{J-1}^n$, where $\nu_0=0.00$ and $\nu_J=8.00$. Fig. 6a shows real and imaginary parts of ${}_0\Gamma_2(\nu,\sqrt{t_M\omega_d})$ in the case of the travel distance $L_2=40$km ($Z_0=100$km) and the difference angular frequency $\omega_d=0.5s^{-1}$ (solid curves) with respect to a initial condition ${}_0\Gamma_2(\nu,0)$ (dashed curves). The value of ${}_0\Gamma_2(0,\sqrt{t_M\omega_d})$ corresponds to the value of ${}_0\Gamma_2(0,z'=L_2,\omega_d,\omega_c)$ or ${}_0\Gamma_2(0,z=Z_0,\omega_d,\omega_c)$. Varying the value of ω_d, we obtain the curve ${}_0\Gamma_2(0,Z_0,\omega_d,\omega_c)$ against ω_d (Fig. 6b). The variation of ${}_0\Gamma_2$ against ω_d depends both on the travel distance and on the random inhomogeneity; the value of ${}_0\Gamma_2$ more rapidly decreases to zero against ω_d at longer travel distance and stronger inhomogeneity. Hence, the appropriate range and step size of ω_d should be taken corresponding to the travel distance and the random inhomogeneity. In general, the value of ${}_0\Gamma_2$ decreases rapidly against ω_d when ω_d is small (see Fig. 6b). Therefore, it is computationally efficient to take small step size when ω_d is small and large step size when ω_d is large.

Substituting the solution ${}_0\Gamma_2(0,Z_0,\omega_d,\omega_c)$ into Eqs. (3.11) and (3.10), we directly synthesize the intensity spectral density $\hat{I}(Z_0,t;\omega_c)$. Since Eq. (3.11) has the form of the Fourier transform, we can use FFT algorithm [17] by interpolating the value of ${}_0\Gamma_2$ with respect to equally spacing ω_d values. Integrating Eq. (3.11) over time, we obtain a conserved value

$$\begin{aligned}\int_{-\infty}^{\infty}\hat{I}_0(z,t;\omega_c)dt&=\int_{-\infty}^{\infty}d\omega_{d0}\Gamma_2(x_d=0,z,\omega_d,\omega_c)\delta(\omega_d)\exp\{i\omega_d z/V_0\}\\&={}_0\Gamma_2(0,z,0,\omega_c)=1,\end{aligned} \tag{3.19}$$

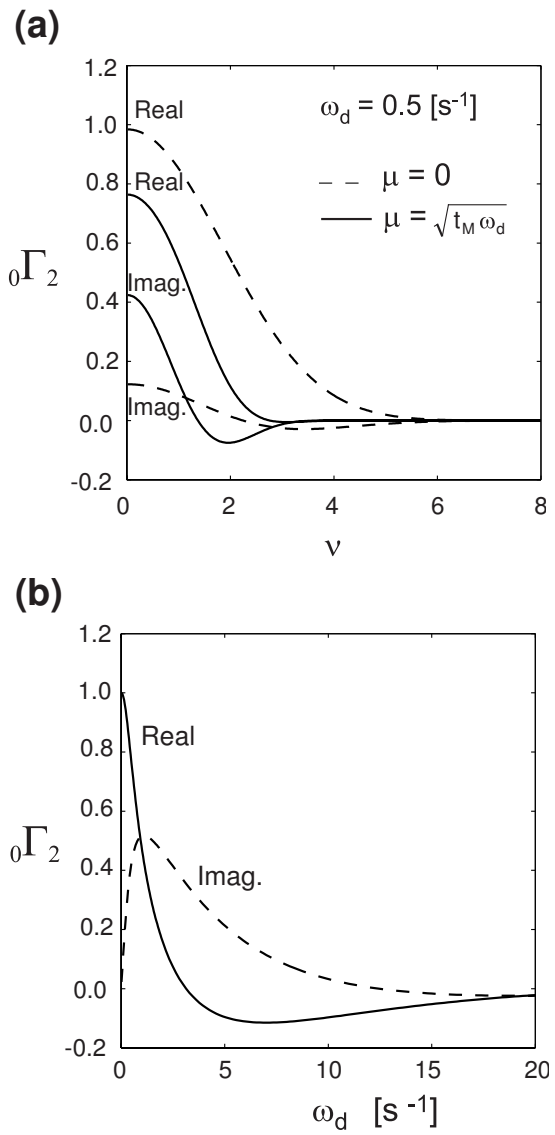

Figure 6: (a) The values of ${}_0\Gamma_2$ against normalized transverse distance ν in the case of difference angular frequency $\omega_d = 0.5\ [s^{-1}]$ in the two-layer random media given by Fig. 2. Real and imaginary parts of an initial condition in Layer 2 are shown by dashed curves, and those of a solution at travel distance $L_2 = 40$km ($z = 100$km) are shown by solid curves. (b) The value of ${}_0\Gamma_2$ against difference angular frequency ω_d for travel distance $L_2 = 40$km ($z = 100$km). Real and imaginary parts are shown by solid and dashed curves, respectively.

since $\partial_0\Gamma_2/\partial z = 0$ when $x_d = 0$ and $\omega_d = k_d V_0 = 0$ [see Eq. (3.12)].

Although we have supposed delta-function type source duration in the above derivation, sources usually have finite duration. In the case of a finite duration source intensity $s(t)$, the corresponding intensity spectral density is obtained by the convolution of $s(t)$

and $\hat{I}(z,t;\omega_c)$. When we set the source intensity as

$$\int_{-\infty}^{\infty} s(t)\,dt = 1,$$

the integral over time of the intensity spectral density function is also conserved,

$$\int_{-\infty}^{\infty} \hat{I}(z,t;\omega_c)\,dt = 1.$$

The envelopes obtained by this method will be referred to as Markov envelopes.

4 Stochastic ray-path method: SR envelopes

In this section, we describe another direct envelope simulation method. Dividing the medium into many thin layers, we interpret wave scattering as a successive ray bending process. The ray bending process is simulated stochastically by using the Monte Carlo method. This idea was proposed by I.P. Williamson [39, 40] and referred to as the stochastic ray-path method. A compact summary is given in [Chapter 6, 36].

4.1 Markov approximation for the mutual coherence function (MCF)

We consider a monochromatic wave with angular frequency ω in Eq. (3.1) and define the mutual coherence function (MCF) at a distance z as a correlation of field U between different locations on the transverse line (x-axis) as

$$\Gamma_1(x',x'',z,\omega) \equiv \langle U(x',z,\omega)\,U(x'',z,\omega)^* \rangle. \tag{4.1}$$

When there exists a length that is larger than a and smaller than the scale of variation of U, neglecting backward scattering, we can derive the master equation for MCF as

$$\frac{\partial \Gamma_1}{\partial z} + k_0^2[A(0) - A(x_d)]\Gamma_1 = 0, \tag{4.2}$$

using the Markov approximation [see p. 244, 28], where the difference coordinate $x_d = x' - x''$ and the function A is the longitudinal integral of ACF defined in Eq. (3.7). Integrating (4.2) for an increment Δz, we have MCF at a distance $z+\Delta z$ as

$$\Gamma_1(x_d,z+\Delta z,k_0) = \Phi(x_d,\Delta z,k_0)\,\Gamma_1(x_d,z,k_0). \tag{4.3}$$

The transfer function is given by

$$\Phi(x_d,\Delta z,k_0) = \exp\left\{-k_0^2[A(0) - A(x_d)]\Delta z\right\}, \tag{4.4}$$

where $\Phi(0,\Delta z,k_0)=1$.

For the incidence of a coherent wave with $\Gamma_1=1$ at $z=0$, using successively (4.3) with an increment Δz, we can get Γ_1 at any distance z. Intensity spectral density $\widehat{I}_0$ is given by the ensemble average of squared amplitude, that is the MCF at $x_d=0$. The Fourier transform of MCF with respect to x_d gives the angular spectrum function (ASF) $\breve{\Gamma}$. Therefore, the intensity spectral density is given by

$$\widehat{I}_0(z;k_0)\equiv\Gamma_1(x_d=0,z,k_0)=\left[\frac{1}{2\pi}\int_{-\infty}^{\infty}dk_x e^{ik_x x_d}\breve{\Gamma}(k_x,z,k_0)\right]_{x_d=0}. \tag{4.5}$$

The ASF $\breve{\Gamma}(k_x,z,k_0)$ is considered as the intensity spectral density propagating with the direction

$$\mathbf{k}=k_x\mathbf{e_x}+\sqrt{k_0^2-k_x^2}\mathbf{e_z},$$

where $\mathbf{e_x}$ and $\mathbf{e_z}$ are unit vectors along the x- and z-axes, respectively. The infinite integration range is formally used in Eq. (4.5) for the Fourier transformation, but in practice, the range of k_x is limited within the range between $-k_0$ and k_0 since we do not consider inhomogeneous waves. Furthermore, the value of $\breve{\Gamma}(k_x,z,k_0)$ rapidly decreases to zero when k_x increases to k_0 since small-angle scattering is supposed. By using the Fourier transform, we may write the master equation (4.3) as a convolution integral for ASF,

$$\breve{\Gamma}(k_x,z+\Delta z,k_0)=\frac{1}{2\pi}\int_{-\infty}^{\infty}dk'_x\,\breve{\Phi}\left(k_x-k'_x,\Delta z,k_0\right)\breve{\Gamma}\left(k'_x,z,k_0\right), \tag{4.6}$$

where the Fourier transform of the transfer function is given by

$$\Phi(x_d,\Delta z,k_0)=\frac{1}{2\pi}\int_{-\infty}^{\infty}dk_x e^{ik_x x_d}\breve{\Phi}(k_x,\Delta z,k_0), \tag{4.7}$$

Eq. (4.6) describes the process of ASF in the thin layer from z to $z+\Delta z$.

Let us introduce new parameter $s\equiv k_x/k_0=\sin\phi$ as an independent variable, where ϕ is the angle of a ray from the z-direction. The value of s varies from -1 to 1 when k_x varies from $-k_0$ to k_0. Since the scattering angle is small or forward scattering is dominant, $k_x\ll k_0$, we may approximate $s\approx\phi$. We re-define the ASF for the parameter s as

$$\breve{\Gamma}_s(s,z,k_0)\equiv\frac{k_0}{2\pi}\breve{\Gamma}(k_0 s,z,k_0)$$

and the transfer function in the s space as

$$\begin{aligned}\breve{\Phi}_s(s,\Delta z,k_0)&\equiv\frac{k_0}{2\pi}\breve{\Phi}(k_0 s,\Delta z,k_0)=\frac{k_0}{2\pi}\int_{-\infty}^{\infty}dx_d\Phi(x_d,\Delta z,k_0)\exp(-ik_0 s x_d)\\&=\frac{1}{2\pi}\int_{-\infty}^{\infty}dw\exp\left\{-k_0^2\left[A(0)-A\left(\frac{w}{k_0}\right)\right]\Delta z\right\}\exp(-isw),\end{aligned} \tag{4.8}$$

where the normalization is

$$\int_{-1}^{1} ds\, \breve{\Phi}_s(s,\Delta z,k_0)=1.$$

The master equation (4.6) is then written as

$$\breve{\Gamma}_s(s,z+\Delta z,k_0)=\int_{-1}^{1} ds'\breve{\Phi}_s(s-s',\Delta z,k_0)\,\breve{\Gamma}_s(s',z,k_0). \tag{4.9}$$

For the case of Gaussian ACF, the longitudinal integral of ACF is given by (3.7), we have $\Phi(x_d,\Delta z,k_0)=\exp\{-\sqrt{\pi}\varepsilon^2\frac{\Delta z}{a}k_0^2x_d^2\}$. It gives a Gaussian-type transfer function as

$$\begin{aligned}\breve{\Phi}_s(s,\Delta z,k_0)&\approx\frac{1}{2\pi}\int_{-\infty}^{\infty}dwe^{-isw}\exp\left\{-\sqrt{\pi}\frac{\varepsilon^2\Delta z}{a}w^2\right\}\\&=\frac{1}{\sqrt{2\pi}\sqrt{\frac{2\sqrt{\pi}\varepsilon^2\Delta z}{a}}}\exp\left\{-\frac{s^2}{2\left(\frac{2\sqrt{\pi}\varepsilon^2\Delta z}{a}\right)}\right\},\end{aligned} \tag{4.10}$$

where the standard deviation

$$\sqrt{2\sqrt{\pi}\varepsilon^2\Delta z/a}$$

is independent of the central frequency.

4.2 Stochastic ray path method

Eqs. (4.9) and (4.10) describe how rays are bent according to the random inhomogeneity in a layer of thickness Δz for stationary state. We may interpret the integral equation (4.9) as a Wiener process where the change in ray direction is stochastically controlled by the spectrum of random media through the transfer function $\breve{\Phi}$. To extend the above solution to non-stationary state problem, we need to calculate the accumulated travel time for each ray path from a source to a receiver.

We divide the random medium into many horizontal layers of thickness Δz as illustrated in Fig. 7. At the n-th boundary, the ray coordinate is (x_n,z_n) and the travel time t_n with small ray angle ϕ_n. Practically we may approximate as

$$s_n\equiv\sin\phi_n\approx\phi_n.$$

After a step increment of Δz in the n-th layer, $z_{n+1}=z_n+\Delta z$,

$$x_{n+1}=x_n+\Delta x_n=x_n+\frac{\Delta z s_n}{\sqrt{1-s_n^2}}\approx x_n+\Delta z\phi_n, \tag{4.11}$$

and the ray path length

$$\Delta l_n=\frac{\Delta z_n}{\cos\phi_n}\approx\Delta z_n\left(1+\frac{\phi_n^2}{2}\right). \tag{4.12}$$

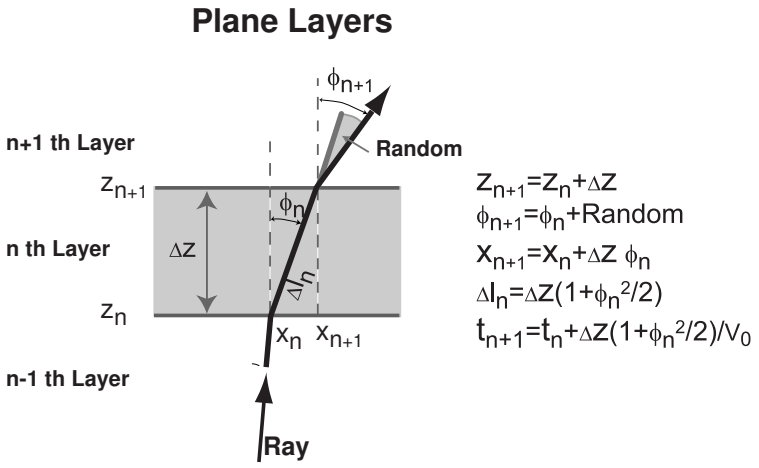

Figure 7: Ray bending process through a plane layer in a random medium.

The travel time is

$$t_{n+1}=t_n+\frac{\Delta l_n}{V_0}\approx t_n+\frac{\Delta z}{V_0}\left(1+\frac{\phi_n^2}{2}\right). \tag{4.13}$$

Stochastic ray bending process is written as

$$\phi_{n+1}=\phi_n+\Delta\phi_n=\phi_n+\text{Random}. \tag{4.14}$$

According to the Monte Carlo method, random angle $\Delta\phi_n=\phi_{n+1}-\phi_n$ is generated by using the transfer function (4.10) as the probability density function for every increment Δz. Since we suppose small-angle scattering, large-angle scattering should be discarded. Considering that $\cos\phi_n\approx 1-{\phi_n}^2/2$ and ϕ_n must be smaller than $\pi/2$, we delimit the range ${\phi_n}^2/2<1$ in this study. The simulation procedure is as follows: first, we shoot many particles from the origin to the z-direction ($s_1=\phi_1=0$) and calculate the travel time of each ray at a target distance $z=Z_0$ according to (4.13). The travel time distribution obtained at the target distance irrespective of their x coordinates represents the time trace of intensity $\widehat{I}_0$ at a central angular frequency ω_c. The finite duration intensity at the source $s(t)$ and the wandering effect $w(t)$ are included by convoluting them with the solution $\widehat{I}_0$. The envelopes obtained by this method will be referred to as SR envelopes.

5 Resultant envelopes and their comparisons

5.1 Uniform random media

Fig. 8a shows a comparison between the Markov envelopes and the SR envelopes in the uniform random media characterized by $\varepsilon=0.04$ and $a=5$km for the incidence of a 2 Hz plane Ricker wavelet. We used the corresponding intensity source time function $s(t)$ for

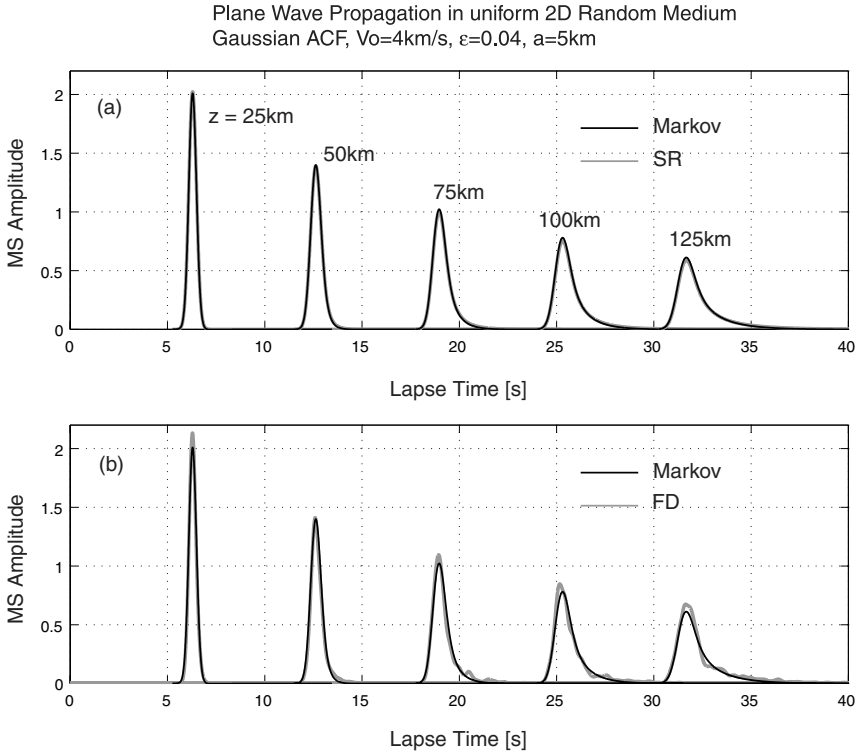

Figure 8: MS envelopes in the uniform random media for the incidence of 2Hz Ricker wavelet. (a) Comparison between the Markov envelopes (black curves) and the SR envelopes based on the stochastic ray-path (gray curves). (b) Comparison between the Markov envelopes (black curves) and the FD envelopes (gray curves).

the convolution. For example, the Markov envelopes at the travel distances at Z_0=75, 100 and 125km are obtained from the values of ${}_0\Gamma_2$ with 2048 grid points of ω_d in the range $[0s^{-1},70s^{-1}]$. The SR envelopes are synthesized with 1,000,000 particles from the source. Those envelopes are in excellent agreement for all the travel distances. Both the Markov envelopes and SR envelopes are based on the parabolic equation, so that their envelopes are almost identical. I. P. Williamson also showed the agreement for 3-D uniform random media [40].

Fig. 8b shows the comparison between the FD envelopes and the Markov envelopes in the uniform random media. In this figure, the SR envelopes are not plotted since they are almost identical to the Markov envelopes. The envelopes of the Markov and the FD simulations are also in good agreement, although there are some slight discrepancies in the later-phase excitation. The Markov envelopes include only small-angle scattering around the forward direction. On the other hand, the FD envelopes rigorously simulate small- and large angle scattering. The discrepancies in the later intensity (intensity at the lapse time around 21s for example), may be due to neglecting large-angle scattering in the Markov envelopes. We note that the difference is small since the small-angle scattering dominates the large-angle scattering in this case.

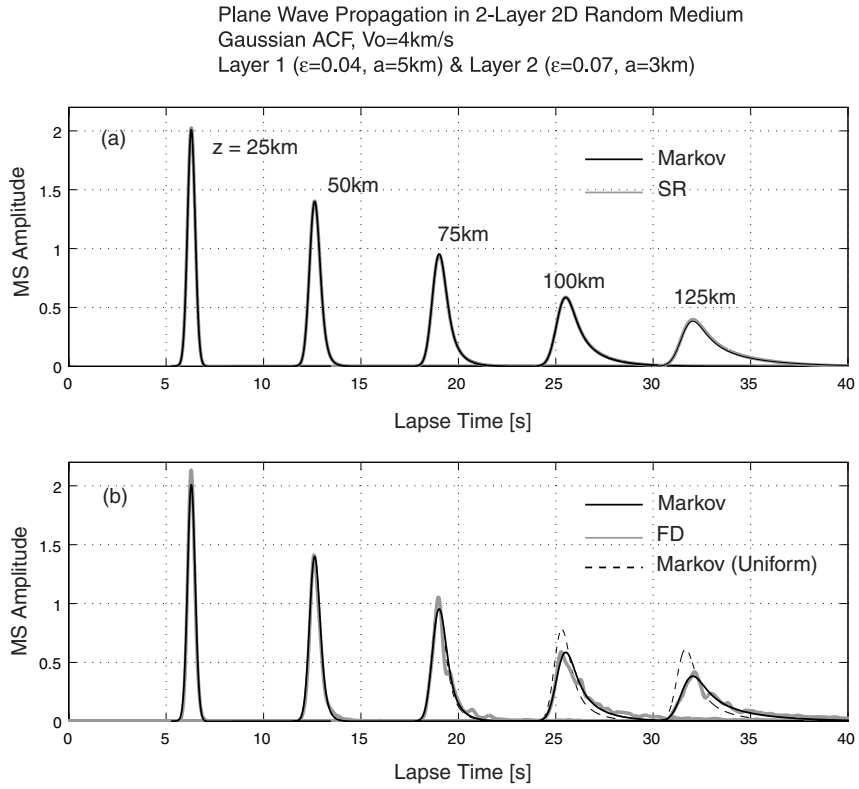

Figure 9: MS envelopes in the two-layer random media for the incidence of 2Hz Ricker wavelet. (a) Comparison between the Markov envelopes (black curves) and the SR envelopes based on the stochastic ray-path (gray curves). (b) Comparison between the Markov envelopes (black curve) and the FD envelopes (gray curves). The Markov envelopes of the uniform random media ($\varepsilon = 0.04$, $a = 5$km, 0km$< z <$160km) are also plotted (dashed curves).

5.2 Two-layer random media

Fig. 9a shows a comparison between the Markov envelopes and SR envelopes in the two-layer random media for the incidence of a 2Hz plane Ricker wavelet. As in the case of the uniform random media (Fig. 8a), those envelopes are in excellent agreement for all travel distances. Note that the stations at the travel distance larger than 60km are located in Layer 2. This study confirms the accordance of the Markov and SR envelopes for non-uniform random media.

Fig. 9b shows a comparison between the Markov envelopes and the FD envelopes for the two-layer random media. The Markov envelopes for the uniform random media are also plotted for the comparison. Since Layer 2 located at the travel distance larger than 60km is characterized as a strong scattering layer, the Markov envelopes for the two-layer random media (solid curves) more rapidly decrease in the maximum amplitude with increasing the travel distance than for the weak uniform media (dashed curves). Also, the

envelopes for the two-layer media (solid curves) have more energy in the later envelope than the envelopes of the weak uniform media (dashed curve). The difference between the envelopes in the two-layer and uniform media increases with increasing the travel distance in Layer 2. The Markov envelopes for the two-layer random media show good accordance with the FD envelopes. This supports the validity of the direct simulation methods, the Markov and the stochastic ray path methods, synthesizing envelopes in the two-layer random media.

6 Summary and discussions

This study presented the scalar wave propagation through two-layer random media composed of weak and strong inhomogeneity zones in 2-D space for the vertical incidence of a plane wavelet. When the wavelength is supposed to be smaller than the characteristic scale of the inhomogeneity, small-angle scattering around the forward direction dominates large-angle scattering. Two direct envelope simulation methods based on the small-angle scattering approximation are examined. One method is to solve a differential equation for the two-frequency mutual coherence function with the Markov approximation. The other is to solve the stochastic ray bending process by using the Monte Carlo method based on the mutual coherence function with the Markov approximation. The resultant wave envelopes of the two methods showed excellent coincidence both for uniform and two-layer random medium cases. We confirmed the validity of these two methods comparing with the envelopes made from the finite difference simulations. The idea that two-layer medium is considered to be the sum of two uniform random media and the connection of the values of TFMCF at the boundary can be easily extended to multi-layer random medium. Also, the synthesis method of SR envelopes is applicable to multi-layer random medium. Although this study dealt with only the case of Gaussian PSDF, it is easy to extend the formulation to a more realistic PSDF having a power-law spectrum [22].

When considering applications of those methods to observed seismograms, one can relate the geometry of plane-wave propagation to teleseismic wave observations. However, we should be careful since the condition $ak \gg 1$ restricts the applicable range to be high frequencies. Extending the plane wave propagation to a point source radiation in 3D space as in the studies [22, 24], our approaches will be applicable to seismograms of local earthquakes. Furthermore, it would be preferable to suppose anisotropic random media characterized by a long horizontal correlation distance compared with the vertical correlation distance, since the anisotropic random media are more realistic to describe lithospheric inhomogeneity [4, 19]. We expect from 2-D study that envelopes in the anisotropic random media are significantly different from those of the isotropic random media [13, 21]. Finally, we should include those extensions in the framework of elastic wave propagation [10, 26, 27]. The formulation and the results in this study would work as a sound mathematical base for those developments.

Acknowledgments

The authors wish to thank M. Korn and J. Kawahara for their valuable comments, which greatly improve this manuscript. We would like to thank those who made efforts to run the high-sensitivity seismograph network Japan (Hi-net).

References

[1] K. Aki and B. Chouet, Origin of coda waves: source, attenuation and scattering effects, J. Geophys. Res., 80 (1975), 3322-3342.
[2] M. Fehler, H. Sato and L.-J. Huang, Envelope broadening of outgoing waves in 2-D random media: A comparison between the Markov approximation and numerical simulations, Bull. Seismol. Soc. Am., 90 (2000), 914-928.
[3] M. Fehler and H. Sato, Coda, Pure Appl. Geophys., 160 (2003), 541-554.
[4] T. Furumura and B. L. N. Kennette, Subduction zone guided waves and the heterogeneity structure of the subducted plate: intensity anomalies in northern Japan, J. Geophys. Res., 110 (2005), B10302, doi:10.1029/2004JB003486.
[5] A. Gusev and I. R. Abubakirov, Vertical profile of effective turbidity reconstructed from broadening of incoherent body-wave pulses. I. General approach and the inversion procedure, Geophys. J. Int., 136 (1999), 295-308.
[6] A. Gusev and I. R. Abubakirov, Vertical profile of effective turbidity reconstructed from broadening of incoherent body-wave pulses. II. Application to Kamchatka data, Geophys. J. Int., 136 (1999), 309-323.
[7] M. Hoshiba, A. Rietbrock, F. Scherbaum, H. Nakahara and C. Haberland, Scattering attenuation and intrinsic absorption using uniform and depth dependent model: application to full seismogram envelope recorded in Northern Chile, J. Seismol., 5 (2001), 157-179.
[8] L.-J. Huang, M. Fehler, P. M. Robert and C. C. Burch, Extended local Rytov Fourier migration method, Geophysics, 64 (1999), 1535-1545.
[9] A. Ishimaru, Wave Propagation and Scattering in Random Media, Academic Press, New York, 1978.
[10] M. Korn and H. Sato, Synthesis of plane vector wave envelopes in two-dimensional random elastic media based on the Markov approximation and comparison with finite-difference simulations, Geophys. J. Int., 161 (2005), 839-848.
[11] L. C. Lee and J. R. Jokipii, Strong scintillations in astrophysics. II. A theory of temporal broadening of pulses, Astrophys. J., 201 (1975), 532-543.
[12] L. Margerin, Introduction to radiative transfer of seismic waves, in: A. Levander and G. Nolet (Eds.), Seismic Earth: Array Analysis of Broadband Seismograms, Geophysical Monograph Series, AGU, Washington, Vol. 157, Ch 14, 2005, pp. 229-252.
[13] L. Margerin, Attenuation, transport and diffusion of scalar waves in textured random media, Tectonophysics, 416 (2006), 229-244.
[14] L. Margerin, M. Campillo and B. A. van Tiggelen, Radiative transfer and diffusion of waves in a layered medium: New insight into coda Q, Geophys. J. Int., 134 (1998), 596-612.
[15] K. Obara and H. Sato, Regional differences of random inhomogeneities around the volcanic front in the Kanto-Tokai area, Japan, revealed from the broadening of S wave seismogram envelopes, J. Geophys. Res., 100 (1995), 2103-2121.

[16] A. G. Petukhin and A. A. Gusev, The Duration-distance relationship and average envelope shapes of small Kamchatka earthquakes, Pure Appl. Geophys., 160 (2002), 1717-1743.
[17] W. H. Press, S. A. Teukolsky, W. T. Vetterling and B. P. Flannery, Numerical Recipes in C, Cambridge University Press, New York, 1987.
[18] J. Przybilla, M. Korn and U. Wegler, Radiative transfer of elastic waves versus finite difference simulations in two-dimensional random media, J. Geophys. Res., 111(B4) (2006), B04305, 10.1029/2005JB003952.
[19] T. Ryberg, M. Tittgemeyer and F. Wenzel, Finite difference modeling of P-wave scattering in the upper mantle, Geophys. J. Int., 141 (2000), 787-800.
[20] S. M. Rytov, Y. A. Kravtsov and V. I. Tatarskii, Principles of Statistical Radio Physics (Vol. 4) Wave Propagation Through Random Media, Springer-Verlag, Berlin, 1989.
[21] T. Saito, Synthesis of scalar-wave envelopes in two-dimensional weakly anisotropic random media using the Markov approximation, Geophys. J. Int., 165 (2006), 501-515.
[22] T. Saito, H. Sato and M. Ohtake, Envelope broadening of spherically outgoing waves in three-dimensional random media having power-law spectra, J. Geophys. Res., 107(B5) (2002), 2089, doi:10.1029/2001JB000264.
[23] T. Saito, H. Sato, M. Fehler and M. Ohtake, Simulating the envelope of scalar waves in 2D random media having power-law spectra of velocity fluctuation, Bull. Seismol. Soc. Am., 93 (2003), 240-252.
[24] T. Saito, H. Sato, M. Ohtake and K. Obara, Unified explanation of envelope broadening and maximum-amplitude decay of high-frequency seismograms based on the envelope simulation using the Markov approximation: Forearc side of the volcanic front in northeastern Honshu, Japan, J. Geophys. Res., 110 (2005), B01304, doi:10.1029/2004JB003225.
[25] H. Sato, Broadening of seismogram envelopes in the randomly inhomogeneous lithosphere based on the parabolic approximation: Southeastern Honshu, Japan, J. Geophys. Res., 94 (1989), 17735-17747.
[26] H. Sato, Synthesis of vector wave envelopes in three-dimensional random elastic media characterized by a Gaussian autocorrelation function based on the Markov approximation: Plane wave case, J. Geophys. Res., 111 (2006), B06306, doi: 10.1029/2005JB004036.
[27] H. Sato, Synthesis of vector wave envelopes in three-dimensional random elastic media characterized by a Gaussian autocorrelation function based on the Markov approximation: Spherical wave case, J. Geophys. Res., (2007), doi: 10.1029/2006JB004437.
[28] H. Sato and M. Fehler, Seismic Wave Propagation and Scattering in the Heterogeneous Earth, Springer-Verlag, New York, 1998.
[29] H. Sato, M. Fehler and T. Saito, Hybrid synthesis of scalar wave envelopes in two-dimensional random media having rich short-wavelength spectra, J. Geophys. Res., 109 (2004), B06303, doi:10.1029/2003JB002673.
[30] F. Scherbaum and H. Sato, Inversion of full seismogram envelopes based on the parabolic approximation: Estimation of randomness and attenuation in southeastern Honshu, Japan, J. Geophys. Res., 96 (1991), 2223-2232.
[31] P. M. Shearer, Introduction to Seismology, Cambridge University Press, Cambridge, 1999.
[32] V. L. Shishov, Effect of refraction on scintillation characteristics and average pulsars, Sov. Astron., 17 (1974), 598-602.
[33] I. A. Sreenivasiah, A. Ishimaru and S. T. Hong, Two-frequency mutual coherence function and pulse propagation in a random medium: An analytic solution to the plane wave case, Radio Sci., 11 (1976), 775-778.
[34] P. L. Stoffa, J. T. Fokkema, R. Freire and W. Kessinger, Split-step Fourier migration, Geo-

physics, 55 (1990), 410-421.
[35] T. Takahashi, H. Sato, T. Nishimura and K. Obara, Strong inhomogeneity beneath Quaternary volcanoes revealed from the peak delay analysis of S-wave seismograms of microearthquakes in northeastern Japan, Geophys. J. Int., 168 (2007), 90-99, doi: 10.1111/j.1365-246X.2006.03197.x.
[36] J. Uscinski, The Elements of Wave Propagation in Random Media, McGraw-Hill, New York, 1977.
[37] U. Wegler, Diffusion of seismic waves in layered media: Boundary conditions and analytical solutions, Geophys. J. Int., 163 (2005), 1123-1135.
[38] U. Wegler, M. Korn and J. Przybilla, Modeling full seismogram envelopes using radiative transfer theory with Born scattering coefficients, Pure Appl. Geophys., 163 (2006), 503-531.
[39] I. P. Williamson, Pulse broadening due to multiple scattering in the interstellar medium, Mon. Not. R. Astron. Soc., 157 (1972), 55-71.
[40] I. P. Williamson, The broadening of pulses due to multi-path propagation of radiation, P. Roy. Soc. Lond. A, 342 (1975), 131-147.
[41] K. Yoshimoto, Monte-Carlo simulation of seismogram envelopes in scattering media, J. Geophys. Res., 105 (2000), 6153-6161.
[42] K. Yoshimoto, U. Wegler and M. Korn, A volcanic front as a boundary of seismic-attenuation structures in northeastern Honshu, Japan, Bull. Seismol. Soc. Am., 96 (2006), 637-646.